UNIVERSITY
OF TRENTO

DIPARTIMENTO DI INGEGNERIA E SCIENZA DELL'INFORMAZIONE

38123 Povo – Trento (Italy), Via Sommarive 14
http://www.disi.unitn.it

LINEAR ARRAY THINNING EXPLOITING ALMOST DIFFERENCE SETS

G. Oliveri, M. Donelli, and A. Massa

January 2011

Technical Report # DISI-11-016

Linear Array Thinning Exploiting Almost Difference Sets

G. Oliveri, M. Donelli, and A. Massa

ELEDIA Research Group

Department of Information and Communication Technologies,

University of Trento, Via Sommarive 14, 38050 Trento - Italy

Tel. +39 0461 882057, Fax +39 0461 882093

E-mail: *andrea.massa@ing.unitn.it*,

{*giacomo.oliveri*, *massimo.donelli*}*@dit.unitn.it*

Web-site: *http://www.eledia.ing.unitn.it*

Linear Array Thinning Exploiting Almost Difference Sets

G. Oliveri, M. Donelli, and A. Massa

Abstract

This paper describes a class of linear thinned arrays with predictable and well-behaved sidelobes. The element placement is based on almost difference sets and the array power pattern is forced to pass through N uniformly-spaced values that, although neither equal nor constant as for difference sets, are *a-priori* known from the knowledge of the aperture size, the number of active array elements K, and the features of the correlation function. Such a property allows one to predict the bounds of the confidence range of the peak sidelobe of the admissible arrays obtainable through simple shift operations on a binary sequence. The expected peak sidelobe performances turn out to be comparable with those from difference sets, even though obtainable in a wider set of array configurations, and improved in comparison with cut-and-try random-placements.

Key words: Array Antennas, Thinned Arrays, Linear Arrays, Almost Difference Sets, Sidelobe Control.

1 Introduction

Massive thinning of arrays (i.e., the reduction of the number of the array elements below half of its filled counterpart) is of great importance in practical applications because of the reduction of the array costs, weight, power consumption, HW and computational complexity [1][2]. However, such advantages usually come at the cost of a loss of sidelobe level (SLL) control and gain compared to the filled arrangement [1][2].

In order to overcome these drawbacks, several thinning techniques have been proposed [1]-[5]. Deterministic thinning has been first studied, but no significant improvements of SLL control compared to a random element placement [4][5] have been obtained. More recently, dynamic programming [6] and stochastic optimization techniques, such as simulated annealing (SA) and genetic algorithms (GAs) have been successfully applied [7]-[11]. Despite the satisfactory results, statistical methodologies have not an easy application to large arrays because of the computational burden and convergence issues. Moreover, due to their stochastic nature, it is often difficult to *a-priori* estimate the expected performances for a given aperture size and thinning factor [1].

The synthesis of massively thinned arrays has been faced in a very promising fashion by considering equally-weighted arrays [1][12]. Such an approach is based on the use of binary sequences derived from *difference sets* (DSs), which are known to possess two-level periodic autocorrelations. In [1][12], it has been shown that, if the element excitations are chosen according to the binary distribution derived from DSs, the peak sidelobe level (PSL) of the synthesized linear array is 3 dB lower than that of the corresponding random distribution. Such a result has been successfully exploited for the design of both linear [13] and planar arrays [1][14], although the PSL reduction is about 1.5 dB smaller when planar architectures are dealt with [1]. The application of DSs has also allowed some improvements in thinned-array design procedures based on GA optimization [2].

The exploitation of DS sequences is a powerful and numerically-effective technique for the thinning of large arrays. However, such a possibility depends on the availability of a DS for whatever size N of the array [1][2][14]. Although several families of DSs have been determined and extensive collections are also available [15], it is well-known that there is no a correspond-

ing DS for several values of N [16] (i.e. it is not possible to define a binary sequence with a two-level periodic autocorrelation of length N).

Recently, the definition of binary sequences of length N with suitable autocorrelation properties, for which DSs are not available, has been carefully investigated in information theory and combinatorial mathematics. It has been found that it is often possible to determine sequences with a three-level autocorrelation function by taking into account the so-called *almost difference sets* (ADSs) [16]-[18]. ADSs are a research topic of great interest in combinatorial theory with important applications in cryptography and coding theory (see [16]-[18] and the references therein). Moreover, although ADS generation techniques are still subject of research, large collections of these sets are already available [22]. As regards the array synthesis, a preliminary application, although limited to a particular subset of ADSs, has been reported in [13]. In such a framework, the whole class of ADSs seem to be a good candidate for enlarging the set of admissible analytic configurations with respect to the DS case, despite a reduction of expected performances. From this viewpoint, it is of interest to carefully detail the ADS features for antenna arrays synthesis.

In this paper, the exploitation of ADSs properties for the design of linear thinned arrays is discussed and analyze in depth through a solid mathematical description. The proposed ADS-based technique is aimed at synthesizing arrays with performances close to those with DSs, but enhancing the set of admissible array configurations. It is also worthwhile to point out that the paper is not aimed at defining an optimal method for the design of thinned arrays, but its purpose is to propose some guidelines to the array designers who, whether by necessity or choice, are synthesizing a thinned array without considering stochastic optimizations or a random placement, but using a deterministic strategy with predictable results.

The outline of the paper is as follows. After a short summary on the basic ADS definitions and properties (Sect. 2), the expected PSL of ADS-arrays is bounded by theoretically defining upper and lower values (Sect. 3) starting from infinite sequences (Sect. 3.1) up to finite arrays (Sect. 3.2). The numerical validation is carried out by comparing the performances of ADS-based arrays with those of similar DS configurations when available and, more in general, with random arrays (Sect. 4). Finally, some representative experiments concerning the exploitation

of ADS-based arrays when non-isotropic elements are at hand is reported (Sect. 4.4). Some conclusions and comments on future developments follow (Sect. 5).

2 Almost Difference Sets - Definitions and Properties

Let us provide just some basic definitions and main properties of ADSs, while more detailed information and applications of ADSs can be found in [16][17][18].

A K-subset $\underline{\mathbf{D}} = \{d_k \in [0,\ N-1]\,,\ d_h \neq d_\ell;\ k,h,\ell = 0,...,K-1\}$ of an Abelian group $\underline{\mathbf{G}}$[(1)] of order N is called a (N,K,Λ,t)-almost difference set if the multiset $\underline{\mathbf{M}} = \{m_j = (d_h - d_\ell),\ d_\ell \neq d_h; j = 0,...,K\times(K-1)-1\}$ contains t nonzero elements of $\underline{\mathbf{G}}$ each exactly Λ times, and the remaining $N-1-t$ nonzero elements each exactly $\Lambda+1$ times [18]. As a consequence, DSs are ADSs for which $t = N-1$ or $t = 0$ [18].

If $\underline{\mathbf{G}} \equiv \mathbb{Z}$ and $\underline{\mathbf{D}}$ is a (N,K,Λ,t)-ADS of $\underline{\mathbf{G}}$, then the cyclic repetition of the binary sequence $\underline{\mathbf{A}} = \{a_n \in [0,\ 1]\,;\ n = 0,...,N-1\}$ of length N, whose n-th element is

$$a_n = \begin{cases} 1 & if \quad n \in \underline{\mathbf{D}} \\ 0 & otherwise \end{cases}\ , \tag{1}$$

defines the characteristic sequence $\underline{\mathbf{S}} = \{s_n;\ n \in \mathbb{Z}\}$ of $\underline{\mathbf{D}}$ [16], where

$$s_n = \begin{cases} 1 & if \quad mod_N(n) \in \underline{\mathbf{D}} \\ 0 & otherwise \end{cases}\ . \tag{2}$$

The corresponding autocorrelation function, $C_s(z)$, is a periodic function defined as follows [1]

$$C_s(z) = \sum_{n=0}^{N-1} s_n s_{n+z} \quad z \in \mathbb{Z} \tag{3}$$

and equal to [16][18]

(1) An Abelian group is a group satisfying the requirement that the product of elements does not depend on their order. In addition to the other axioms of a group, the product operation is associative, $\underline{\mathbf{G}}$ has an identity element, and every element of $\underline{\mathbf{G}}$ has an inverse.

$$C_s^{ADS}(z) = \begin{cases} K & z = 0 \\ \Lambda + 1 & z \in \underline{\mathbf{L}} \\ \Lambda & otherwise \end{cases}, \quad K \geq \Lambda + 1 \tag{4}$$

in the period $z \in [0,\ N-1]$, $\underline{\mathbf{L}}$ being a set of $N-1-t$ elements (i.e., $\underline{\mathbf{L}} = \{l_p \in \mathbb{Z};\ p = 1, ..., N-1-t\}$).

For illustrative purposes, let us consider the examples of ADSs [17] reported in Tab. I together with the corresponding binary sequences and autocorrelation functions. For completeness, the plots of $C_s^{ADS}(z)$ are shown in Fig. 1.

It is worth noting that the autocorrelation function $C_s^{ADS}(z)$ of a (N, K, Λ, t)-ADS is close to that of the (if any) corresponding (N, K, Λ)-DS [1]

$$C_s^{DS}(z) = \begin{cases} K & z = 0 \\ \Lambda & otherwise \end{cases}. \tag{5}$$

In fact, the difference is limited to just a unity in $N-1-t$ points where $C_s^{ADS}(z) = \Lambda + 1$ [16][18]. Moreover, the ADSs share several other properties with the DSs. In particular, neither DS nor ADS can be defined for every value of N, K, Λ and t. Indeed, for (N, K, Λ, t)-ADSs in an Abelian group, the following existence condition holds true [17][18]

$$K(K-1) = t\Lambda + (N-1-t)(\Lambda+1) \tag{6}$$

being $K \geq \Lambda + 1$, $0 \leq K \leq N$, and $0 \leq t \leq N-1$.

On the other hand, if $\underline{\mathbf{D}}$ is an ADS, then the set

$$\underline{\mathbf{D}}^{(\sigma)} = \left\{ d_k^{(\sigma)} = mod_N\left(d_k + \sigma\right),\ d_h \neq d_\ell;\ k, h, \ell = 0, ..., K-1 \right\} \tag{7}$$

where $\sigma \in \mathbb{Z}$, is still an ADS. Therefore, starting from an (N, K, Λ, t)-ADS, it is possible to build N different (N, K, Λ, t)-ADSs by applying a cyclic shift to its elements (i.e., a cyclic shift on the associated binary sequence $\underline{\mathbf{A}}$).

Mathematical proofs of existence or non-existence of ADSs for different choices of N are

currently topic of research in the framework of combinatorial theory and suitable techniques for the generation of new families of ADSs are still in progress [18]. However, several ADSs has been already found [16]-[18] and their properties can be profitably exploited for array synthesis.

3 ADS-Based Linear Arrays - Mathematical Formulation

3.1 ADS-based Infinite Arrays

An infinite thinned array can be defined from whatever binary sequence $\underline{\mathbf{A}}$ of length N by introducing the *array element location function* $\Psi_\infty(x)$ [1]

$$\Psi_\infty(x) = \sum_{n=-\infty}^{\infty} s_n \delta(x - nd) \tag{8}$$

where $\delta(\,.\,)$ is the Dirac delta function, d and x are the lattice spacing and the spatial coordinate along the linear array, respectively (both expressed in wavelength). In practice, the infinite thinned array is defined by locating the array elements along a uniform lattice with spacing d [1] at those positions where $\Psi_\infty(x) \neq 0$.

As with any array, the power pattern of the ADS-based infinite linear array turns out to be the Fourier transform of the autocorrelation function of $\Psi_\infty(x)$ [1], $C_\Psi^{ADS}(z)$, that is

$$PP_\infty(u) = \mathcal{F}\left\{C_\Psi^{ADS}(z)\right\} \tag{9}$$

where $\mathcal{F}\{\,.\,\}$ denotes the Fourier transform operator, $u \triangleq sin(\theta)$, $u \in [-1, 1]$, and

$$C_\Psi^{ADS}(z) = \Lambda \sum_{n=-\infty}^{\infty} \delta(z - nd) + \sum_{p=1}^{N-1-t} \left\{ \sum_{n=-\infty}^{\infty} \delta(z - nNd - l_p d) \right\} + (K - \Lambda) \sum_{n=-\infty}^{\infty} \delta(z - nNd) \tag{10}$$

where the index l_p satisfies the condition $C_s\,(l_p) = \Lambda + 1$.

By substituting (10) in (9) and recalling the Fourier transformation properties of an infinite train of pulse functions, one can show that

$$PP_\infty(u) = \sum_{n=-\infty}^{\infty} PP_{\infty,n} \delta\left(u - \frac{n}{Nd}\right) \tag{11}$$

where

$$PP_{\infty,n} = \begin{cases} \frac{\Lambda}{d} + \frac{1}{Nd}\left(K - \Lambda + \sum_{p=1}^{N-1-t} e^{j\frac{2\pi l_p n}{N}}\right) & n = 0, \pm N, \pm 2N, ... \\ \frac{1}{Nd}\left(K - \Lambda + \sum_{p=1}^{N-1-t} e^{j\frac{2\pi l_p n}{N}}\right) & otherwise \end{cases} . \quad (12)$$

Expression (11) is the analogous of Eq. (14) in [1] for DSs. However, unlike DSs, further simplifications of Eq. (11) are not trivial since the following term of $PP_{\infty,n}$

$$\left(K - \Lambda + \sum_{p=1}^{N-1-t} e^{j\frac{2\pi l_p n}{N}}\right) = \left(K - \Lambda - 1 + \sum_{p=0}^{N-1-t} e^{j\frac{2\pi l_p n}{N}}\right), \quad l_0 = 0 \quad (13)$$

cannot be evaluated in closed form. In fact, the set $\underline{\mathbf{L}}$ depends on the ADS at hand and $PP_{\infty}(u)$ has to be evaluated on a case-by-case basis instead of in a general fashion. However, it is still possible to provide an *a-priori* estimate of the peak sidelobe level of the infinite array, PSL_{∞}, defined as

$$PSL_{\infty} = max_{n \neq 0} \frac{PP_{\infty,n}}{PP_{\infty,0}}. \quad (14)$$

Actually, it turns out that (Appendix A) PSL_{∞} is limited by the following upper

$$PSL_{\infty}^{MAX} = \frac{K - \Lambda - 1 + \sqrt{t\,(N-t)}}{(N-1)\,\Lambda + K - 1 + N - t} \quad (15)$$

and lower bounds

$$PSL_{\infty}^{MIN} = \frac{K - \Lambda - 1 - \sqrt{\frac{t(N-t)}{(N-1)}}}{(N-1)\,\Lambda + K - 1 + N - t}, \quad (16)$$

respectively. Figure 2 shows the plots of the PSL_{∞} values and the corresponding bounds in correspondence with the representative set $\underline{\mathbf{D}}_4$ available in [17] and detailed in Tab. I. As expected, $PSL_{\infty}^{MIN}\left(\underline{\mathbf{D}}^{(\sigma)}\right) \leq PSL_{\infty}\left(\underline{\mathbf{D}}^{(\sigma)}\right) \leq PSL_{\infty}^{MAX}\left(\underline{\mathbf{D}}^{(\sigma)}\right)$[(2)] since [$PSL_{\infty}^{MAX}\left(\underline{\mathbf{D}}_4^{(\sigma)}\right) = -11.59$ dB, $PSL_{\infty}\left(\underline{\mathbf{D}}_4^{(\sigma)}\right) = -14.29$ dB, $PSL_{\infty}^{MIN}\left(\underline{\mathbf{D}}_4^{(\sigma)}\right) = -18.03$ dB]. Moreover, for fixed values of $\eta \triangleq \frac{t}{N-1}$ and of the thinning percentage factor ν, ($\nu \triangleq \frac{K}{N}$), the range of variation of PSL_{∞} reduces as N increases until a threshold. Such a behavior is pointed out in the pictures reported

[(2)] Please notice that for an infinite ADS-based array: $PSL_{\infty}\left(\underline{\mathbf{D}}^{(\sigma)}\right) = PSL_{\infty}\left(\underline{\mathbf{D}}^{(0)}\right)$ since every $\underline{\mathbf{D}}^{(\sigma)}$ generates the same power pattern $PP_{\infty}(u)$.

in Fig. 3 that summarizes the results of a study on the dependence of the confidence range index $\Delta_\infty \triangleq \frac{PSL_\infty^{MAX}}{PSL_\infty^{MIN}}$, which by Eqs. (6), (15), and (16) turns out to be (see Appendix 3)

$$\Delta_\infty = \frac{N^2(\nu-\nu^2) - \eta N + \eta + (N-1)\sqrt{N^2(\eta-\eta^2) + N(2\eta^2-\eta) - \eta^2}}{N^2(\nu-\nu^2) - \eta N + \eta - (N-1)\sqrt{N(\eta-\eta^2) + \eta^2}}, \qquad (17)$$

on N for different values of the ADS-parameters. The asymptotic threshold of Δ_∞ appears to be equal to

$$lim_{N\to\infty}\left(\Delta_\infty\right) = \frac{\nu - \nu^2 + \sqrt{\eta\left(1-\eta\right)}}{\nu - \nu^2}. \qquad (18)$$

As expected, the condition $\Delta_\infty = 0$ dB is asymptotically verified when $\eta = 1$ (i.e., $t = N-1$ and the ADS coincides with a DS), since $PSL_\infty = PSL_\infty^{DS}$ [Eq. (19) in [1]] [see Fig. 3(*a*) - "dashed brown curve"]. Such a conclusion identically holds true for $\eta = 0$ (i.e., $t = 0$), whatever the admissible value of ν (see Fig. 3(*a*) - $\nu = 0.5$). Figure 3 also confirms that $\Delta_\infty\left(\eta\right) = \Delta_\infty\left(1-\eta\right)$ starting from a threshold value N_η, which decreases from $N_{\eta\to 1.0} = \infty$ as $\eta \to 0.5$.

As far as Figure 3(*b*) is concerned, neither the plots with $\nu = 0$ (i.e., $K = 0$ - Empty array) nor those concerning $\nu = 1.0$ (i.e., $K = N$ - Filled array) are considered since they do not admit a three-level autocorrelation function as needed for ADSs. Let us also notice from Eq. (17) that the following property $\Delta_\infty\left(\nu\right) = \Delta_\infty\left(1-\nu\right)$ holds true as pointed out in by the plots in Fig. 3(*b*). Moreover, the analysis and the corresponding plots are limited to the range of N values for which an ADS sequence can exist [i.e., (6), $K \geq \Lambda+1$, $0 \leq K \leq N$, and $0 \leq t \leq N-1$]. As it can be observed, the value of the confidence index decreases when $|\nu - 0.5| \to 0$ and it attains its minimum value when $\nu = 0.5$. In such a case, $\Delta_\infty \to \left[1 + 4\sqrt{\eta\left(1-\eta\right)}\right]$ asymptotically with a maximum value equal to $max_\eta\left\{\Delta_\infty\rfloor_{\nu=0.5}\right\} \approx 4.77$ dB for $\eta = 0.5$ [Fig. 3(*b*)].

3.2 ADS-Based Finite Arrays

As regards finite arrays, since the *array element location function* $\Psi(x)$

$$\Psi(x) = \sum_{n=0}^{N-1} s_n \delta(x - nd) \qquad (19)$$

is now a truncated version of $\Psi_\infty(x)$, then it can be easily shown that $PP_\infty(u)$ and the power pattern of the finite configuration, $PP(u)$, are related by the following relationship [1]

$$PP_\infty(u) = PP(u)\frac{\sum_{n=-\infty}^{\infty}\delta\left(u-\frac{n}{Nd}\right)}{Nd}. \tag{20}$$

Accordingly, $PP(u)$ necessarily satisfies the sampling condition at each coordinate $u = u_n = \frac{n}{Nd}$ [1], that is

$$PP(u_n) = N\,d\,PP_{\infty,n}, \quad n = 0, ..., \left\lfloor \frac{N}{2} \right\rfloor. \tag{21}$$

In order to illustrate such a behavior, Figure 4 shows the plots of $PP(u)$ and of the coefficients $PP_{\infty,n}$ for the thinned array of $K = 22$ elements on a $N = 45$-locations lattice ($d = \frac{1}{2}$) defined from the ADS $\underline{\mathbf{D}}_4$ [16]. It is worth noting that, since $\Psi(x)$ is real-valued, the beampattern is symmetric with respect to $u = 0$ and only the range $u \in [0, 1]$ is considered.

Staring from (20), it is then possible to estimate the PSL of a finite array

$$PSL \triangleq \frac{max_{u\in\left[U_M\left(\underline{\mathbf{D}}^{(\sigma)}\right),1\right]}\left\{PP\left(u\right)\right\}}{PP\left(0\right)} \tag{22}$$

where U_M is the width of the mainlobe region, by using the associated infinite array power pattern $PP_\infty(u)$. It is worth noting that (see Fig. 4) the PSL value is determined by the behaviour of the power pattern at $u = u_{m+\frac{1}{2}} = \frac{(m+\frac{1}{2})}{Nd}$ [1]

$$PSL = \frac{max_m\left\{PP\left(u_{m+\frac{1}{2}}\right)\right\}}{PP\left(0\right)}, \quad m = 1, ..., \left\lfloor \frac{N}{2} \right\rfloor \tag{23}$$

being $u_{m+\frac{1}{2}} = \frac{(m+\frac{1}{2})}{Nd}$.

To evaluate $PP(u_{m+\frac{1}{2}})$, let us consider the sampling theorem [12][19] and (20). It follows that

$$PP(u) = \left|\sum_{n=0}^{N-1}\sqrt{N\,d\,PP_{\infty,n}}e^{j\phi_n}\frac{sin\left[\pi Nd\left(u-\frac{n}{Nd}\right)\right]}{Nsin\left[\pi d\left(u-\frac{n}{Nd}\right)\right]}\right|^2 \tag{24}$$

where ϕ_n, $n = 0, ..., N-1$, are the phase terms of the sampled array factor ($\phi_0 = 0$) [1], which are known quantities only when the ADS at hand is specified [1]. By evaluating (24) in $u = 0$

and $u = u_{m+\frac{1}{2}}$ and substituting in (23), we obtain

$$PSL = \frac{max_m \left\{ \left| \sum_{n=0}^{N-1} \sqrt{PP_{\infty,n}} e^{j\phi_n} \frac{\sin[\pi(m-n+\frac{1}{2})]}{N \sin[\pi(m-n+\frac{1}{2})/N]} \right|^2 \right\}}{PP_{\infty,0}}, \quad m = 1, ..., \left\lfloor \frac{N}{2} \right\rfloor. \tag{25}$$

Consequently, the PSL of an ADS-based *finite* array is fully specified from the knowledge of $PP_{\infty,n}$ and ϕ_n, $n = 0, ..., N-1$. However, since the $PP_{\infty,n}$ coefficients of ADS sequences neither can be expressed in closed-form (as for RDSs [13]) nor have equal expressions (as for DSs [1]), it is not available (although approximated) a threshold value for the PSL as for DSs [1] [Eq. (40)]. Nevertheless, it is possible to yield (see Appendix B) the following set of inequalities

$$PSL^{MIN} \leq PSL^{DW} \leq PSL^{opt} \leq PSL^{UP} \leq PSL^{MAX} \tag{26}$$

where $PSL^{opt} = min_{\sigma \in [0,N-1]} \left\{ PSL\left(\underline{\mathbf{D}}^{(\sigma)}\right) \right\}$, $PSL^{MIN} = PSL_{\infty}^{MIN}$, $PSL^{DW} = max\left\{PSL_{\infty}, PSL^{min}\right\}$, $PSL^{UP} = E\left\{\Phi_N^{min}\right\} PSL_{\infty}$, and $PSL^{MAX} = E\left\{\Phi_N^{min}\right\} PSL_{\infty}^{MAX}$, being $E\left\{\Phi_N^{min}\right\} \approx 0.8488 + 1.128\, log_{10} N$ and $PSL^{min} = E\left\{\Phi_N^{min}\right\} \frac{min_n(PP_{\infty,n})}{PP_{\infty,0}}$. In should be pointed out that PSL^{DW} and PSL^{UP} are determined when the ADS sequence is available since they require the knowledge of the coefficients $PP_{\infty,n}$. On the contrary, PSL^{MIN} and PSL^{MAX} can be always *a-priori* computed from (16) and (15), respectively.

For a preliminary check of the reliability of (26), let us consider the finite arrays coming from the ADSs $\underline{\mathbf{D}}_1$ and $\underline{\mathbf{D}}_2$ in Tab. I. The PSL values of the ADS-based finite arrays deduced from these ADSs and their cyclic shifts are given in Fig. 5 and compared with the PSL confidence ranges, while the associated PPs are reported in Fig. 6. As expected, the value of the PSL changes when the ADS is cyclically shifted of σ positions (Fig. 5), although each power pattern always passes through the fixed points at $u = u_n = \frac{n}{Nd}$ (Fig. 6). Notwithstanding, the PSL^{opt} lies into the confidence range prescribed by (26). Such a value is yielded for different shift values (Fig. 5), pointing out that less than N trials/shifts are needed to identify a "good" (i.e., a solution within the bounds *a-priori* known) ADS configuration with negligible computational costs.

4 Numerical Analysis

This section is devoted to numerically assess the potentialities and limitations of the ADS-based array thinning theory for antenna synthesis. A comparative study is carried out and some experiments concerning directional arrays (i.e., arrays with directive elements) are reported to point out features and characteristics of the ADS-based deterministic thinning.

For fair comparisons, let us consider as reference random arrays and DS-based placements for which beam pattern performances can be *a-priori* envisaged [3] as for ADS-based configurations. More specifically, the estimator of the normalized peak sidelobe level of *random arrays* $(RND)^{(3)}$ is equal to [3]

$$PSL_{RND} = \frac{B + 1 + \frac{2}{B}}{K} \tag{27}$$

where $B = -ln\left[1 - \beta^{\frac{\lambda}{d(N-1)}}\right]$, β being the probability or confidence level that no sidelobe exceeds the PSL_{RND} value. Moreover, the random placement of the array elements on a lattice enables a further reduction of the PSL compared to random arrays [1]

$$PSL_{RNL} = (1 - \nu)\, PSL, \tag{28}$$

although it becomes vanishingly small with increased thinning (i.e., $\nu \to 0$).

Figures 8 and 9 summarize the behaviors of the PSL bounds for both random and ADS-based finite arrays versus the array aperture in correspondence with a set of representative thinning values and for $\eta = 0.5$. Figure 9 also shows the estimated PSL bounds versus η when $N = 45$, the value of PSL_4^{opt}, and the associated optimal power pattern. Likewise ADS curves and because of the asymptotic nature of the random array theory [3], PSL_{RND} and PSL_{RNL} are plotted only for values of K large enough to guarantee that Eqs. (27)-(29) provide satisfactory estimates [3]. More specifically, the minimum value of K to have a reliable estimation of the PSL in random arrays is equal to [3]

(3) *Random arrays* are characterized by element locations chosen by random processes. Generally, they are designed starting from filled configurations and removing at random a given fraction of the elements. Moreover, a *random lattice* array is an array in which the elements are located at randomly chosen positions in a set of uniformly-spaced points (called *lattice*) in the aperture.

$$K_{RND} = max\left\{15,\, 2B\right\}. \tag{29}$$

On the other hand, it should be pointed out that the estimator of the PSL of random arrays is evaluated, instead of the power ratio of the average sidelobe to the main lobe, since this latter may be somewhat misleading and the arising prediction, given by $E\left\{PSL_{RND}\right\} = \frac{1}{K}$, inadequate due to possible significant differences with PSL_{RND} [3].

As it can be observed, although the 3 dB improvement of DS arrays does not verify, the ADS upper bound PSL^{MAX} is always lower than PSL_{RNL} ($PSL_{RNL} \leq PSL_{RND}$) except for highly filled large arrays [Fig. 8(*c*) - $\nu = 0.8$, $N \gtrsim 450$]. On the other hand, it should be noticed that the PSL^{MAX} value usually overestimates the actual peak sidelobe of the ADS array. Such a behavior is pointed out by the PSL values actually obtained from a set of ADSs-based arrays in [22] for which $\eta = \nu = 0.5$ [Fig. 7(*b*)]. A further assessment is also given by the sample at $N = 45$ in Fig. 8(*a*) and pictorially shown in Fig. 8(*b*) where the plot of the corresponding power pattern is drawn.

As regards the confidence index Δ ($\Delta \triangleq \frac{PSL^{MAX}}{PSL^{MIN}}$), similar conclusions to those obtained when dealing with infinite ADS arrays (Sect. 3.1) hold true, but the ADS values are shifted of $E\left\{\Phi_N^{min}\right\}$ since $\Delta = E\left\{\Phi_N^{min}\right\}\Delta_\infty$. The plots in Fig. 7(*d*) assess such a behavior when dealing with large apertures ($N = 10^4$). As a matter of fact, Δ still decreases as $|\nu - 0.5| \to 0$ with a minimum value for $\nu = 0.5$ [Fig. 7(*b*)].

As far as the dependence of the PSL on the index η is concerned, the results in Fig. 9, where the behavior of the PSL bounds versus η and for different values of N and ν is pictorially described, and Fig. 8(*c*) further confirm the indications on the reliability of the ADS-based design. The ADS peak sidelobe turns out to be still lower than those coming from random placements. Moreover, one should notice that the worst situation takes place in correspondence with $\eta = 0.5$, further strengthening and extending to different η values the indications drawn from Fig. 7 ($\eta = 0.5$) about the efficiency of ADS arrays over the random ones. Furthermore, the PSL^{MAX} tends to the DS value when $\eta = 0$ and $\eta = 1$ ($N \to \infty$) as shown in Fig. 9 and Fig. 8(*c*).

Figure 8(*c*) also points out that the actual value of $PSL\left(\underline{\mathbf{D}}_4^{opt}\right)$ is quite close to that predicted

by Eq. (40) in [1] for the admissible (i.e., theoretically existing, but whose explicit form is not yet available) DS array $\underline{\mathbf{E}}_4^{opt}$ with equal number of elements N and thinning percentage ($\nu = 0.489$). This event suggests that using ADSs for array thinning can provide, besides a wider set of admissible array configurations, PSL performances which are expected on average to be close to those from equivalent (i.e., $\eta = 0.0$ or $\eta = 1.0$) or similar (i.e., $N^{ADS} \approx N^{DS}$, $K^{ADS} \approx K^{DS}$, and $\Lambda^{ADS} \approx \Lambda^{DS}$) DS sequences.

In order to point out such an issue, let us compare the pattern features of the finite arrays generated from the sequences $\underline{\mathbf{D}}_2^{(\sigma)}$ and $\underline{\mathbf{E}}_2^{(\sigma)} = \{1+\sigma,\ 3+\sigma,\ 13+\sigma,\ 16+\sigma,\ 17+\sigma\}$, $\sigma = 0, ..., N-1$; $N = 21$ (derived from the $(21, 5, 1)$-DS in [15] with a cyclic shift by 10). Figures 10(*a*) and 10(*b*) show the normalized power patterns of the optimal finite arrays obtained by cyclic shifting the corresponding binary sequences, while Figs. 10(*c*)-10(d) provide the PSLs and beamwidth U_M versus σ of the arrays. The pattern values at the control points $u = u_n$, $n = 0, ..., \left\lfloor \frac{N}{2} \right\rfloor$, where $PP(u_n)\rfloor_{\underline{\mathbf{D}}_2^{(\sigma)}} = N\, d\, PP_{\infty,n}^{ADS}$ and $PP(u_n)\rfloor_{\underline{\mathbf{E}}_2^{(\sigma)}} = N\, d\, PP_{\infty,n}^{DS}$ are reported in Figure 10(*a*), as well. As expected, the best DS-based array slightly overcomes its ADS counterpart only in terms of array beamwidth [Fig. 10(*d*)], while equal PSL values appear [Fig. 10(*c*)].

On the other hand, it is worthwhile to note that the radiation pattern from $\underline{\mathbf{D}}_2^{opt}$ has lower sidelobes in the angular range near the mainlobe [see Fig. 10(*b*)]. Such a feature of ADS placements [see also the plot of $PP(u)\rfloor_{\underline{\mathbf{D}}_3^{opt}}$ in Fig. 11(*c*)] can be profitably exploited when directive array elements are at hand. For instance and likewise [7], let us consider a $cos(\theta)$ element pattern and ideal conditions by neglecting mutual coupling effects. In such a case, the radiated array power pattern is obtained by the product of the isotropic array pattern with the element pattern [2][7]. As it can be seen [Fig. 10(*b*)] and confirmed by the values of the quantitative pattern indexes in Figs. 10(*c*)-10(*d*), the PSL of the directional array in correspondence with $\underline{\mathbf{D}}_2^{opt}$ turns out to be of about 1 dB smaller that that of the isotropic DS-based array, despite the use of low-directive elements and starting from the same PSL value of the the isotropic case.

Such a possibility is not related to a particular test case or a very-special element pattern, but it is due to the distribution of the even-numbered samples of the power pattern that assume only two-constant values for DS-arrays, while multiple levels when dealing with ADS-based

configurations. Therefore, the DS patterns are asymptotically ($N \rightarrow \infty$) constrained to the constant value $PP^{DS}_{\infty,n}$, $n \neq 0$. On the contrary, the variability of the ADS samples admits some (even non-negligible) variations both in the angular range of a pattern [see the isotropic curves in Fig. 10(*b*) and Fig. 11(*c*)] and among different patterns related to the same ADS sequence (Fig. 4 and Fig. 6).

Unlike DS coefficients, the fact that $PP^{ADS}_{\infty,n}$, $n \neq 0$, are not constant provides an additional degree of freedom to the design of thinned arrays through ADS sequences. In fact, besides the possibility to easily find the optimal ADS-based finite array through simple cyclic sequence shift, the availability of different ADS patterns with various characteristics [Fig. 11(*a*) - PSL value; Fig. 11(*b*) - Beamwidth, U_M] depending on σ can be further profitably exploited to minimize the sidelobes of the array power pattern outside the main lobe of the element pattern. The arising effect is then to reduce the number of sidelobes which can compete to the PSL and, by properly selecting a $\underline{\mathbf{D}}^{(\sigma)}$ sequence, the resulting peak sidelobe level of the whole array keeping or decreasing the array beamwidth U_M. Towards this end, it turns out to be more convenient to choose the cyclic ADS-based array with the minimum sidelobe level in the region near the mainlobe and not that with the lowest PSL in the whole angular range as for isotropic elements.

For illustrative purposes, let us consider the test case concerning $\underline{\mathbf{D}}_3$ (Fig. 11). Despite the minimum PSL of the isotropic array is obtained for $\sigma = 15 - 18$, the best directional array in terms of peak sidelobe level comes from a different ADS shift (i.e., $\sigma = 14$) indicated as $\underline{\mathbf{D}}_3^{dir}$ in the following and defined as

$$\underline{\mathbf{D}}_3^{dir} = arg\left\{min_{\sigma\in[0,N-1]}\left[max_{u\in\left[U_M\left(\underline{\mathbf{D}}_3^{(\sigma)}\right),1\right]}\left(PP(u)\rfloor_{\underline{\mathbf{D}}_3^{(\sigma)}}\left[1-u^2\right]\right)\right]\right\}. \qquad (30)$$

As it can be seen, the improvement allowed by the use of directive elements is enough to minimize the sidelobe peaks in the angular region far from the main lobe, thus reducing the arising PSL also in comparison with the directive pattern generated from $\underline{\mathbf{D}}_3^{opt}$ (i.e., $\underline{\mathbf{D}}_3^{opt} = arg\left\{min_{\sigma\in[0,N-1]}\left[max_{u\in\left[U_M\left(\underline{\mathbf{D}}_3^{(\sigma)}\right),1\right]}\left(PP(u)\rfloor_{\underline{\mathbf{D}}_3^{(\sigma)}}\right)\right]\right\}$).

Finally, the performances expected by thinned arrays designed using ADSs are compared with

those from robust stochastic optimization techniques based on GAs [7][9][8][2]. Towards this end, an array of $N = 200$ elements is used as benchmark test case. Figure 12 shows the ADS bounds when $\eta = 0.5$ (i.e., the worst case for ADSs) and the PSL values of the arrays synthesized with the GA-based methods. Moreover, the PSL of the arrangement defined by the ADS $(197, 147, 109, 98)$ [22] is reported, as well. As it can be observed, $PSL^{MIN} < PSL_{GA} < PSL^{MAX}$, PSL_{GA} referring to the GA-optimized designs. Moreover, the ADS-based array favorably compares in terms of PSL with the state-of-the-art GA arrays despite its slightly smaller aperture (197 elements versus 200).

5 Conclusions and Discussion

In this paper, the thinning of linear arrays has been studied by exploiting the properties of ADSs to provide some guidelines for the design of thinned arrays with predictable performances. Such a deterministic approach is not aimed at obtaining optimal designs, but at being applied either when stochastic optimizers or random placement techniques cannot be applied or to speed up the convergence to optimal thinning solutions of optimization techniques. In fact, evolutionary or statistical techniques (e.g., GAs, SA, and PSO) could be computationally expensive when dealing with very large or massively thinned arrays. Moreover, their performances in terms of pattern features of the arising placements are difficult to predict *a-priori*. On the other hand, cut-and-try variations of the element locations in random arrays usually require several trials before providing the satisfactory results expected from random theory.

Unlike standard synthesis techniques, the proposed methodology exploits the properties of ADSs rather than using a search algorithm for the placement of the array elements within a regular lattice. Such a deterministic thinning does not require search or minimization or trial-and-error procedures, but it determines the array arrangement just through simple shifts of suitable sequences. Moreover, the array performances are *a-priori* estimated thanks to the analytic features of the arising ADS-based power patterns. Thanks to these outcomes, the final results of the research work is the description of a practical design theory where the key-role descriptive design parameters are in evidence as well as their impact on the array performances.

From the numerical analysis, it appears that likewise DS placements, but in a theoretically

wider admissible set of configurations, the ADS array performances definitely overcome those of their random counterparts except for large almost filled arrays. In these cases, the actual improvement has to be evaluated on a case-by-case basis and it cannot be assured in advance without the knowledge of the ADS sequence.

A detailed comparison of ADS-based arrays with stochastically-thinned solutions (e.g., GA-based [7] or SA-based arrays [10][11]) is postponed to future researches. Certainly, it seems to be convenient to hybridize the two approaches in some a way and, for example, as suggested in [1] dealing with DSs and shown in [2] with quite satisfactory results.

Future works will be also devoted to find new explicit ADS sequences, but such a topic is out-of-the-scope of the present paper since not pertinent to antenna arrays, but concerning combinatorial mathematics.

Appendix A

This appendix is aimed at determining the range of variation of the PSL of ADS-based infinite arrays. Therefore, let us determine the upper bound and the lower one for PSL_∞. Towards this end, let us first notice that the real [(I)] coefficient $\mathcal{B}_n = \sum_{p=0}^{N-1-t} e^{j\frac{2\pi l_p n}{N}}$ defines the discrete Fourier transform (DFT) of the binary sequence $\underline{\mathbf{B}} = \{b_m;\, m = 0, ..., N-1\}$

$$\mathcal{B}_n = DFT\left\{\underline{\mathbf{B}}\right\} \tag{31}$$

where $b_m = 1$ if $m \in \{\underline{\mathbf{L}} \cup l_0\}$ and $b_m = 0$ otherwise. Therefore, the value of PSL_∞ depends on $\underline{\mathbf{B}}$ and since

$$\mathcal{B}_0 = N - t, \tag{32}$$

it turns out that

$$PSL_\infty = \frac{K - \Lambda - 1 + max_{n\neq 0}\left\{\mathcal{B}_n\right\}}{(N-1)\,\Lambda + K - 1 + N - t}. \tag{33}$$

[(I)] It can be proved that $\mathcal{B}_n \in \mathbb{R}$, since $PP_{\infty,n}$ is real-valued as a sample of the power pattern and the other terms in the right-hand side of (12) are still real quantities.

Let us now observe that, from the Parseval's theorem [19], the "energy" of the sequence $\underline{\mathbf{B}}$ ($\mathcal{E}_B \triangleq \sum_{n=0}^{N-1} |\mathcal{B}_n|^2$) is a constant value

$$\mathcal{E}_B = N \sum_{m=0}^{N-1} |b_m|^2 = N\ (N-t)\,, \tag{34}$$

then the bounds for PSL_∞ are obtained when the following conditions hold true: (*a*) $PSL_\infty = PSL_\infty^{MAX}$ if only one $\mathcal{B}_n = \mathcal{B}^{MAX}$ ($n \neq 0$) is non null; (*b*) $PSL_\infty = PSL_\infty^{MIN}$ if $\mathcal{B}_n = -\hat{\mathcal{B}}$, $n = 1, ..., N-1$. Moreover, the Blahut's theorem [20][21] states that the number of non-null coefficients $\mathcal{B}_n$, $n = 0, ..., N-1$ is equal to the linear span[(II)] of $\underline{\mathbf{B}}$.

As regards the upper bound PSL_∞^{MAX}, the condition (*a*) verifies in correspondence with the non-trivial $\underline{\mathbf{B}}$ having the shortest linear span. Such a binary sequence is obtained when $\underline{\mathbf{L}}$ is a collection of even integers

$$\underline{\mathbf{L}} = \{l_p = 2 \times p;\ p = 1, ..., N-1-t\}\,. \tag{35}$$

In such a case, thanks to the Blahut's theorem [20], it results that

$$\mathcal{E}_B = |\mathcal{B}_0|^2 + \left|\mathcal{B}^{MAX}\right|^2. \tag{36}$$

Therefore, by substituting (32) and (34) in (36) and considering (33), one obtains

$$PSL_\infty^{MAX} = \frac{K - \Lambda - 1 + \mathcal{B}^{MAX}}{(N-1)\,\Lambda + K - 1 + N - t} \tag{37}$$

being $\mathcal{B}^{MAX} = \sqrt{t\,(N-t)}$.

As far as PSL_∞^{MIN} is concerned, the condition (*b*) holds true when the linear span of $\underline{\mathbf{B}}$ is maximum (i.e., N). Such condition corresponds to the case in which a constant energy is

[(II)] The linear span of a binary sequence of period N is defined as the order of the least order homogeneous linear recursion satisfied by the binary sequence. In practice, it can be identified as the size of the smallest linear feedback shift register that generates the sequence. It represents a measure of the complexity of the binary sequence.

forced in the sidelobe region. Consequently,

$$\hat{\mathcal{B}} = \sqrt{\frac{\mathcal{E}_B - |\mathcal{B}_0|^2}{N-1}} = \sqrt{\frac{t\,(N-t)}{(N-1)}}, \tag{38}$$

then

$$PSL_{\infty}^{MIN} = \frac{K - \Lambda - 1 - \hat{\mathcal{B}}}{(N-1)\,\Lambda + K - 1 + N - t} \tag{39}$$

under the condition that $K - \Lambda - 1 > \hat{\mathcal{B}}$.

Appendix B

This section is devoted to derive (26).

As far as the upper bound for the PSL of a finite ADS-based array is concerned, let us consider that $PP_{\infty,n} \leq max_n\,(PP_{\infty,n})$, $n = 1, ..., N-1$, therefore

$$PSL^{(\sigma)} \leq max_{m=1,...,\lfloor \frac{N}{2} \rfloor} \left\{ \left| \frac{(-1)^m}{N sin\left[\frac{\pi\left(m+\frac{1}{2}\right)}{N}\right]} + \sqrt{PSL_{\infty}} \sum_{n=1}^{N-1} \frac{(-1)^{m-n}\, e^{j\phi_n^{(\sigma)}}}{N sin\left[\frac{\pi\left(m-n+\frac{1}{2}\right)}{N}\right]} \right|^2 \right\}, \tag{40}$$

where $PSL^{(\sigma)} = PSL\left(\underline{\mathbf{D}}^{(\sigma)}\right)$. In the *sidelobe region*$^{(III)}$ of $PP\,(u)$, it is possible to approximate the right side of (40) to obtain the following

$$PSL^{(\sigma)} \lesssim PSL_{\infty} max_{m=1,...,\lfloor \frac{N}{2} \rfloor} \left\{ \left| \sum_{n=1}^{N-1} \frac{(-1)^{m-n}\, e^{j\phi_n^{(\sigma)}}}{N sin\left[\frac{\pi\left(m-n+\frac{1}{2}\right)}{N}\right]} \right|^2 \right\}. \tag{41}$$

Let us now model the phase terms $\phi_n^{(\sigma)}$, $n = 1, ..., N-1$, as independent random variables with uniform probability function over the whole angular range. Then, analogously to the treatment

$^{(III)}$ The *sidelobe region* is defined as the angular range $u \in \left[U_M\left(\underline{\mathbf{D}}^{(\sigma)}\right),\, 1\right]$ where the first term in (40) is negligible.

in [1], it can be deduced that

$$PSL^{(\sigma)} \lesssim \Phi^{(\sigma)}\, PSL_{\infty} \tag{42}$$

$\Phi^{(\sigma)}$ being another random variable defined as

$$\Phi^{(\sigma)} = \left| \sum_{n=-\infty}^{\infty} \frac{e^{j\phi_n^{(\sigma)}}}{\left[\pi\left(n-\frac{1}{2}\right)\right]} \right|^2 . \tag{43}$$

However, it should be noticed that we are interested in defining threshold values for $PSL^{opt} = min_{\sigma\in[0,N-1]}\left\{PSL^{(\sigma)}\right\}$. Accordingly, it turns out that

$$PSL^{opt} \lesssim PSL_{\infty}\Phi_N^{min} \tag{44}$$

where $\Phi_N^{min} \triangleq min_{\sigma\in[0,N-1]}\left\{\Phi^{(\sigma)}\right\}$ has an average value equal to

$$E\left\{\Phi_N^{min}\right\} \approx 0.8488 + 1.128\, log_{10}\left(N\right) \tag{45}$$

for sufficiently large values of N [1]. Finally, by also exploiting (15), one obtains that

$$PSL^{opt} \lesssim PSL_{\infty}\, E\left\{\Phi_N^{min}\right\} \leq PSL_{\infty}^{MAX}\, E\left\{\Phi_N^{min}\right\}. \tag{46}$$

With reference to the lower bound for the PSL, let us observe that the power pattern of a finite ADS-based array (whatever the cycling shift) must necessarily pass through the sampling points at $u_n = \frac{n}{Nd}$. Therefore, the corresponding PSL cannot be smaller than the maximum value of $PP\left(u_n\right) = Nd \times PP_{\infty,n}$. Accordingly and also taking into account (16), the following inequality must be satisfied

$$PSL^{(\sigma)} \geq PSL_{\infty} \geq PSL_{\infty}^{MIN}. \tag{47}$$

Such a condition can be further detailed by considering the same proof guidelines used for the PSL upper bound and the condition that $PP_{\infty,n} \geq min_n\left(PP_{\infty,n}\right)$, $n = 0, ..., N-1$. It follows

that

$$PSL^{(\sigma)} \gtrsim \frac{min_n\left(PP_{\infty,n}\right)}{PP_{\infty,0}}\, max_{m=1,\ldots,\left\lfloor\frac{N}{2}\right\rfloor}\left\{\left|\sum_{n=1}^{N-1}\frac{(-1)^{m-n}\, e^{j\phi_n^{(\sigma)}}}{Nsin\left[\frac{\pi\left(m-n+\frac{1}{2}\right)}{N}\right]}\right|^2\right\} \tag{48}$$

and by introducing the random variable Φ_N^{min}, we obtain

$$PSL^{opt} \gtrsim E\left\{\Phi_N^{min}\right\}\frac{min_n\left(PP_{\infty,n}\right)}{PP_{\infty,0}}. \tag{49}$$

Finally, by suitably merging (47) and (49), the lower bound condition states that

$$PSL^{opt} \geq max\left\{PSL_\infty,\, E\left\{\Phi_N^{min}\right\}\frac{min_n\left(PP_{\infty,n}\right)}{PP_{\infty,0}}\right\} \geq PSL_\infty^{MIN}. \tag{50}$$

Appendix C

This section is aimed at deriving (17).

Starting from Eqs. (15) and (16) we have that

$$\Delta_\infty = \frac{K-\Lambda-1+\sqrt{t\left(N-t\right)}}{K-\Lambda-1-\sqrt{\frac{t(N-t)}{(N-1)}}}, \tag{51}$$

where Λ can be expressed as follows

$$\Lambda = \frac{K(K-1)+t+1-N}{N-1} = \frac{\nu^2N^2+N(\eta-\nu-1)+1-\eta}{N-1} \tag{52}$$

by using (6) and recalling that $K=\nu N$ and $t=\eta(N-1)$. Finally, Equation (17) is obtained by simple algebra substituting (52) in (51).

References

[1] D. G. Leeper, “Isophoric arrays - massively thinned phased arrays with well-controlled sidelobes,” *IEEE Trans. Antennas Propag.*, vol. 47, no. 12, pp. 1825-1835, Dec 1999.

[2] S. Caorsi, A. Lommi, A. Massa, and M. Pastorino, “Peak sidelobe reduction with a hybrid approach based on GAs and difference sets,” *IEEE Trans. Antennas Propag.*, vol. 52, no. 4, pp. 1116-1121, Apr. 2004.

[3] B. Steinberg, “The peak sidelobe of the phased array having randomly located elements,” *IEEE Trans. Antennas Propag.*, vol. 20, no. 2, pp. 129-136, Mar. 1972.

[4] B. Steinberg, “Comparison between the peak sidelobe of the random array and algorithmically designed aperiodic arrays,” *IEEE Trans. Antennas Propag.*, vol. 21, no. 3, pp. 366-370, May 1973.

[5] K. C. Kerby and J. T. Bernhard, “Sidelobe level and wideband behavior of arrays of random subarrays,” *IEEE Trans. Antennas Propag.*, vol. 54, no. 8, pp. 2253-2262, Aug. 2006.

[6] S. Holm, B. Elgetun, and G. Dahl, “Properties of the beampattern of weight- and layout-optimized sparse arrays,” *IEEE Trans. Ultrason., Ferroelectr., Freq. Control*, vol. 44, no. 5, pp. 983-991, Sep. 1997.

[7] R. L. Haupt, “Thinned arrays using genetic algorithms,” *IEEE Trans. Antennas Propag.*, vol. 42, no. 7, pp. 993-999, Jul. 1994

[8] R. L. Haupt, D. H. Werner, *Genetic algorithms in electromagnetics*. Hoboken, NJ: Wiley, 2007.

[9] D. S. Weile and E. Michielssen, “Integer-coded Pareto genetic algorithm design of antenna arrays,” *Electron. Lett.*, vol. 32, pp. 1744-1745, 1996.

[10] A. Trucco and V. Murino, “Stochastic optimization of linear sparse arrays,” *IEEE J. Ocean Eng.*, vol. 24, no. 3, pp. 291-299, Jul. 1999.

[11] A. Trucco, “Thinning and weighting of large planar arrays by simulated annealing,” *IEEE Trans. Ultrason., Ferroelectr., Freq. Control*, vol. 46, no. 2, pp. 347-355, Mar. 1999.

[12] D. G. Leeper, “Thinned periodic antenna arrays with improved peak sidelobe level control,” U.S. Patent 4071848, Jan. 31, 1978.

[13] L. E. Kopilovich and L. G. Sodin, “Linear non-equidistant antenna arrays based on difference sets,” *Sov. J. Commun. Technol. Electron.*, vol. 35, no. 7, pp. 42-49, 1990.

[14] L. E. Kopilovich, “Square array antennas based on hadamard difference sets,” *IEEE Trans. Antennas Propag.*, vol. 56, no. 1, pp. 263-266, Jan. 2008.

[15] La Jolla Cyclic Difference Set Repository (*http://www.ccrwest.org/diffsets.html*).

[16] C. Ding, T. Helleseth, and K. Y. Lam, “Several classes of binary sequences with three-level autocorrelation,” *IEEE Trans. Inf. Theory*, vol. 45, no. 7, pp. 2606-2612, Nov. 1999.

[17] K. T. Arasu, C. Ding, T. Helleseth, P. V. Kumar, and H. M. Martinsen, “Almost difference sets and their sequences with optimal autocorrelation,” *IEEE Trans. Inf. Theory*, vol. 47, no. 7, pp. 2934-2943, Nov 2001.

[18] Y. Zhang, J. G. Lei, and S. P. Zhang, “A new family of almost difference sets and some necessary conditions,” *IEEE Trans. Inf. Theory*, vol. 52, no. 5, pp. 2052-2061, May 2006.

[19] A. B. Carlson, P. B. Crilly, and J. C. Rutledge, *Communication Systems*. San Francisco: McGraw-Hill, 2001.

[20] R. Blahut, “Transform techniques for error-control codes,” *IBM J. Res. Develop.*, vol. 23, pp. 299-315, 1979.

[21] M. Goresky, A. M. Klapper, and L. Washington, “Fourier transforms and the 2-adic span of periodic binary sequences," *IEEE Trans. Inf. Theory*, vol. 46, no. 2, pp. 687-691, Mar 2000.

[22] ELEDIA Almost Difference Set Repository (*http://www.ing.unitn.it/~eledia/html/*).

FIGURE CAPTIONS

- **Figure 1.** Autocorrelation function $C_s^{ADS}(z)$ of $\underline{\mathbf{D}}_1$ and $\underline{\mathbf{D}}_2$ in Tab. I.

- **Figure 2.** Plots of $PSL_\infty\,(\underline{\mathbf{D}})$, its bounds $PSL_\infty^{MAX}\,(\underline{\mathbf{D}})$ and $PSL_\infty^{MIN}\,(\underline{\mathbf{D}})$, and of $PP_{\infty,n}\,(\underline{\mathbf{D}})$ for the infinite arrays derived from the ADS $\underline{\mathbf{D}} = \underline{\mathbf{D}}_4$ in Tab. (I).

- **Figure 3.** Plot of Δ_∞ versus the array dimension, N, when: (*a*) $\nu = 0.5$ - $\eta \in [0,\,1]$ and (*b*) $\eta = 0.5$ - $\nu \in [0,\,1]$.

- **Figure 4.** Normalized $PP(u)$s derived from the ADS $\underline{\mathbf{D}}_4$ (i.e., $\underline{\mathbf{D}}_4 = \underline{\mathbf{D}}_4^{(\sigma)}\Big\rfloor_{\sigma=0}$) and its cyclic shifts $\underline{\mathbf{D}}_4^{(\sigma)}$ ($\sigma = 17$, $\sigma = 24$). Number of elements: $N = 45$ - Aperture size: 22λ.

- **Figure 5.** PSL values of the ADS-finite arrays generated from the sequences $\underline{\mathbf{D}}_i^{(\sigma)}$, $\sigma = 0, ..., N-1$: (*a*) $i = 1$ - $N = 13$, and (*b*) $i = 2$ - $N = 21$.

- **Figure 6.** Normalized $PP(u)$s of the ADS-finite arrays generated from the sequence $\underline{\mathbf{D}}_i^{(\sigma)}$, $\sigma = 0, ..., N-1$: (*a*) $i = 1$ - $N = 13$ and (*b*) $i = 2$ - $N = 21$.

- **Figure 7.** *Comparative Assessment* - Plots of the PSL bounds of the ADS-based finite arrays and of the estimator of the PSL of random arrays (RND - random array, RNL - random lattice array) versus the array dimension, N, when (*a*) $\nu = 0.3$, (*b*) $\nu = 0.5$, and (*c*) $\nu = 0.8$. Plots of the confidence ranges of ADS-based arrays versus the thinning index ν when $\eta = 0.5$ and $N = 10^4$ (*d*).

- **Figure 8.** *Comparative Assessment* - Plots of the PSL bounds of the ADS-based finite arrays and of the estimator of the PSL of the random arrays (RND - random array, RNL - random lattice array) when $\nu = 0.489$ versus (*a*) the array dimension, N, and (*c*) the index η. Normalized $PP(u)$ generated from $\underline{\mathbf{D}}_4^{opt}$ and estimated PSL values of the corresponding random sequences (*b*).

- **Figure 9.** *Comparative Assessment* - Plots of the PSL bounds of the ADS-based finite arrays, of the estimator of the PSL of random arrays (RND - random array, RNL - random lattice array), and values of the PSL of DS-based finite arrays versus η when (*a*) $\nu = 0.3$, (*b*) $\nu = 0.5$, and (*d*) $\nu = 0.8$.

- **Figure 10.** *Non-Isotropic Elements* - Finite arrays generated from the ADS-sequences $\underline{\mathbf{D}}_2^{(\sigma)}$ and the DS-sequences $\underline{\mathbf{E}}_2^{(\sigma)}$, $\sigma = 0, ..., N-1$; $N = 21$. Optimal $PP(u)$s radiated from the arrays with (*a*) isotropic elements and (*b*) directive radiators. Pattern features versus σ: (*c*) PSL and (*d*) U_M ($\times \times \times$ Isotropic array; ——— Directional array).

- **Figure 11.** *Non-Isotropic Elements* - Finite arrays generated from the ADS-sequences $\underline{\mathbf{D}}_3^{(\sigma)}$, $\sigma = 0, ..., N-1$; $N = 33$. Pattern features: (*a*) PSL and (*b*) U_M. Normalized $PP(u)$s of the ADS-finite arrays generated from the sequences $\underline{\mathbf{D}}_3^{opt}$ and $\underline{\mathbf{D}}_3^{dir}$ by using isotropic and directive elements.

- **Figure 12.** *Comparative Assessment* - Plots of the PSL bounds of the ADS-based finite arrays ($\eta = 0.5$) and of the estimator of the PSL of random arrays (RND - random array, RNL - random lattice array) versus ν when $N = 200$. PSL values of the arrays genetically optimized in [7] ($N = 200$), [9] ($N = 200$), [2] ($N = 200$) and of the ADS-based array [22] ($N = 197$).

TABLE CAPTIONS

- **Table I.** Examples of ADSs and their descriptive functions.

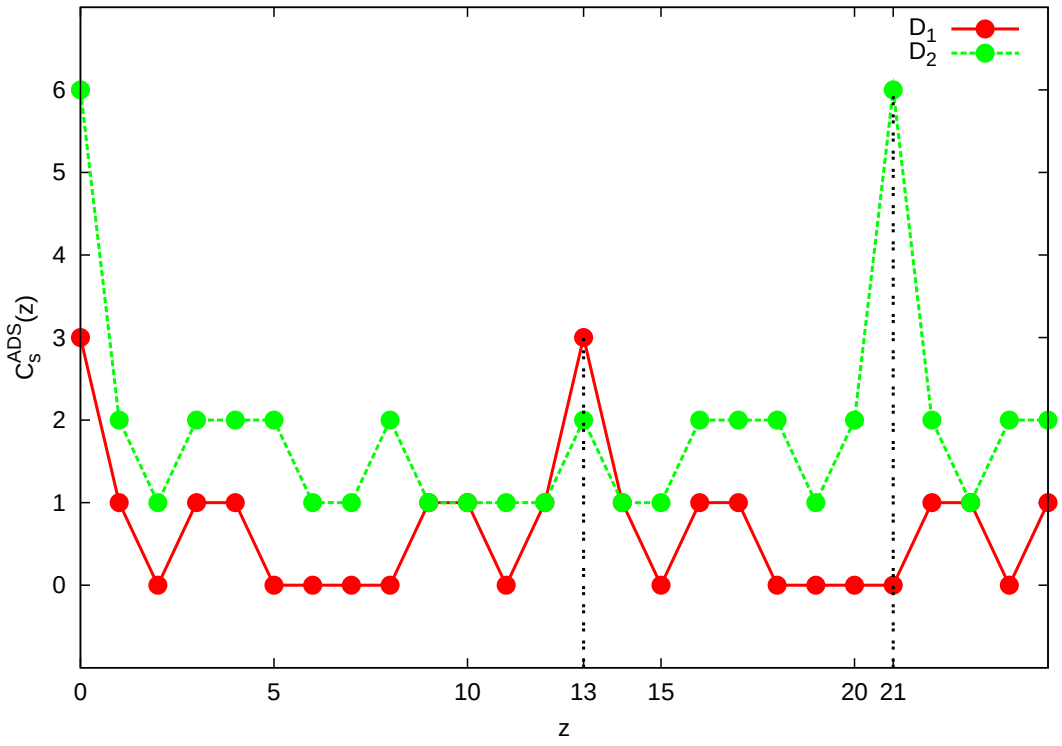

Figure 1 - G. Oliveri et *al.*, “Linear array thinning ...”

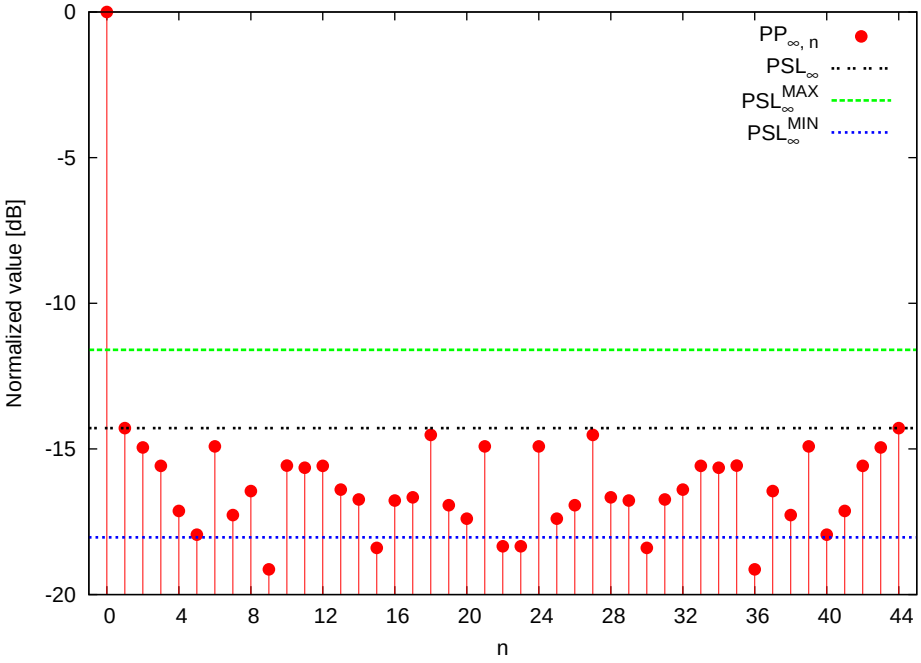

Figure 2 - G. Oliveri et *al.*, “Linear array thinning ...”

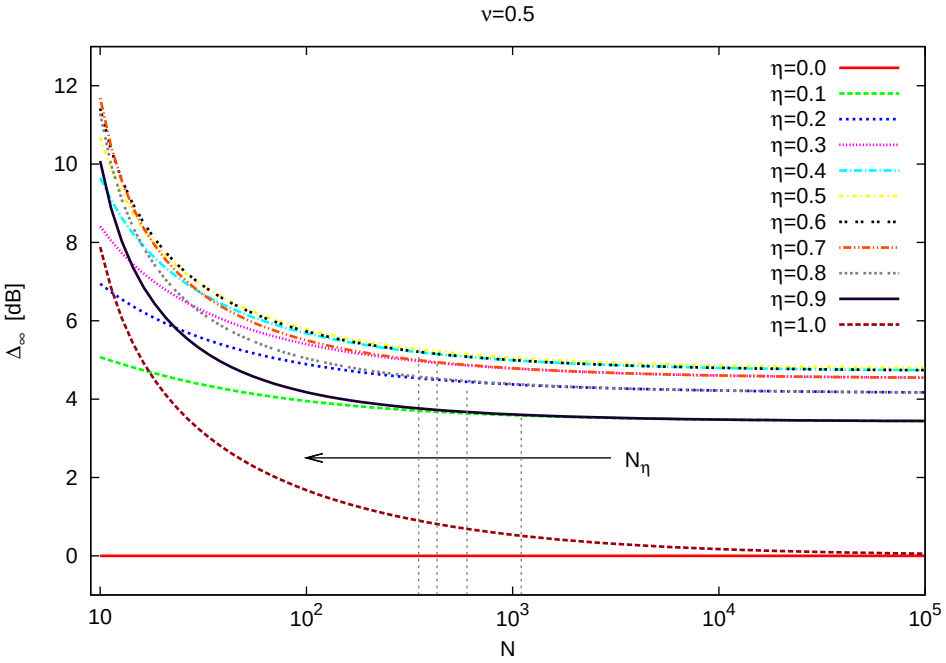

(*a*)

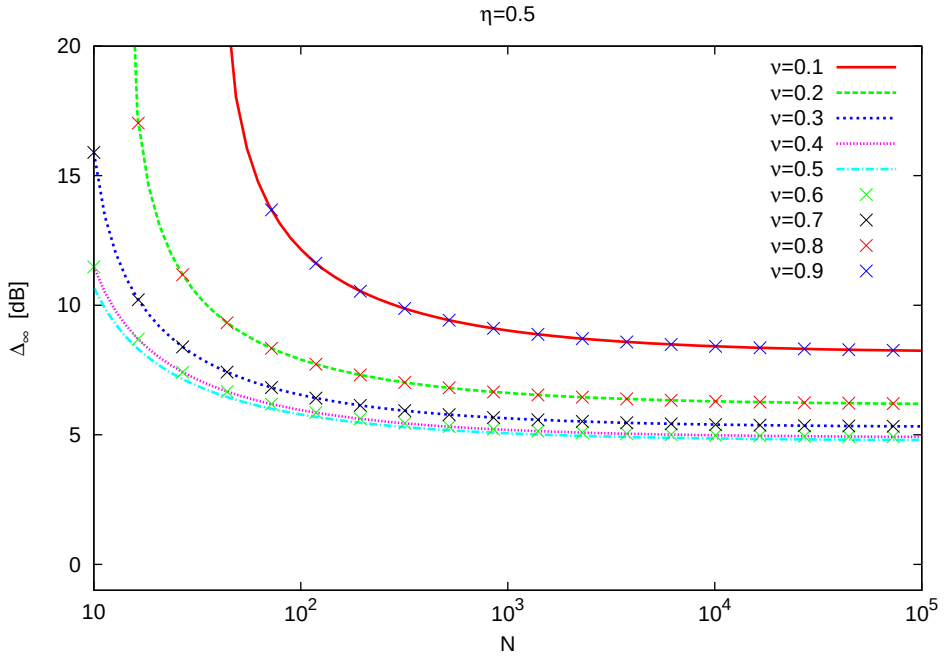

(*b*)

Figure 3 - G. Oliveri et *al.*, “Linear array thinning ...”

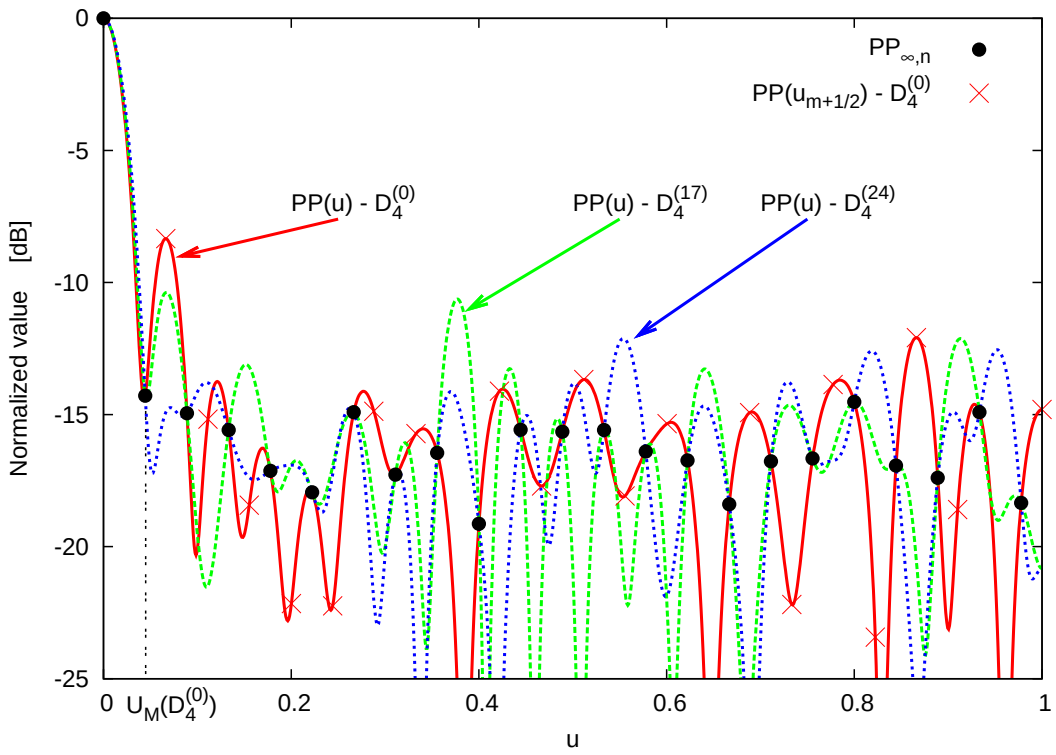

Figure 4 - G. Oliveri et *al.*, "Linear array thinning ..."

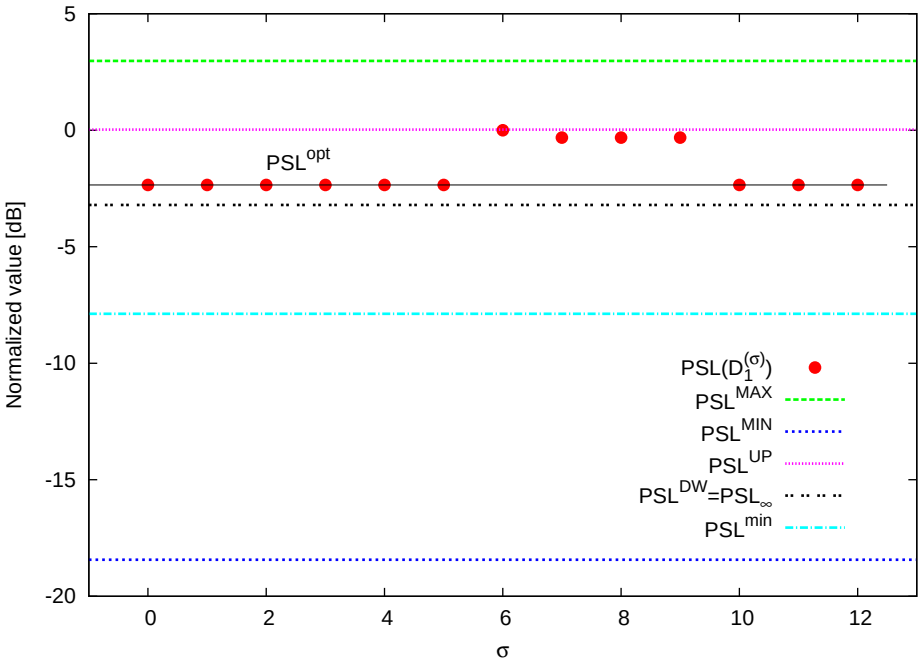

(*a*)

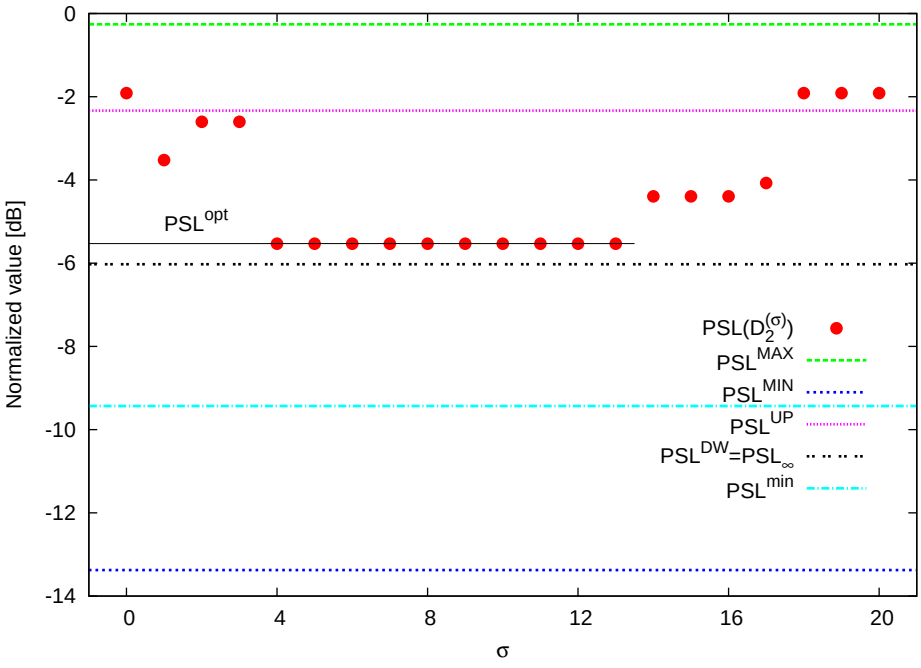

(*b*)

Figure 5 - G. Oliveri et *al.*, "Linear array thinning ..."

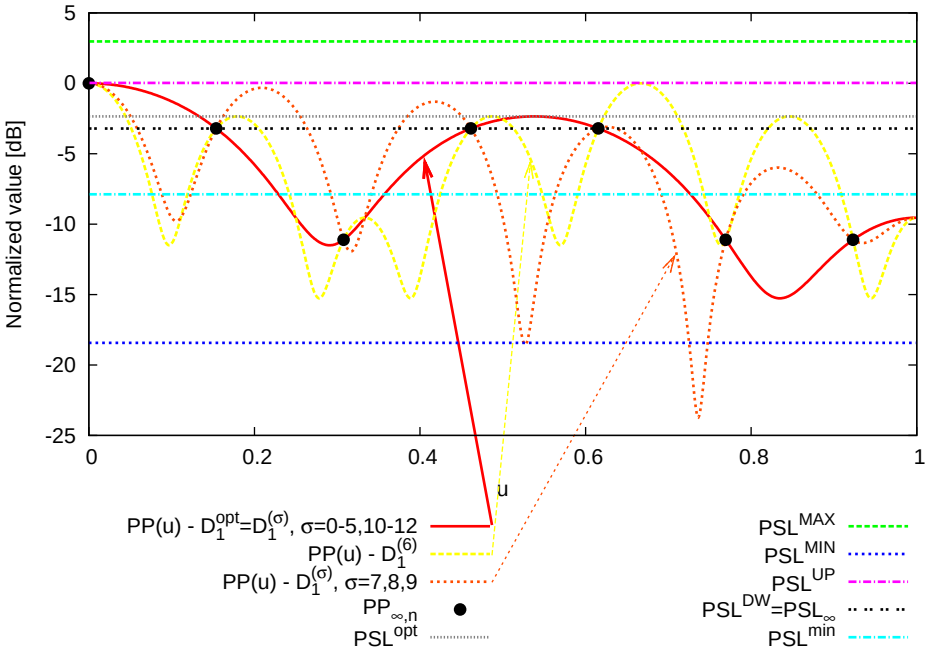

(*a*)

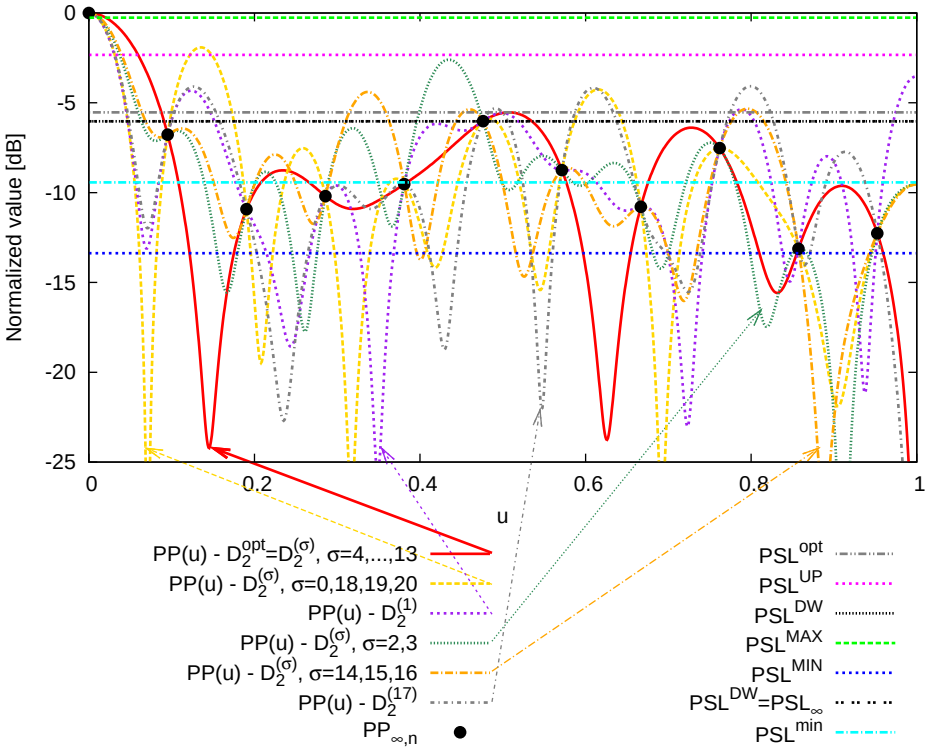

(*b*)

Figure 6 - G. Oliveri et *al.*, “Linear array thinning ...”

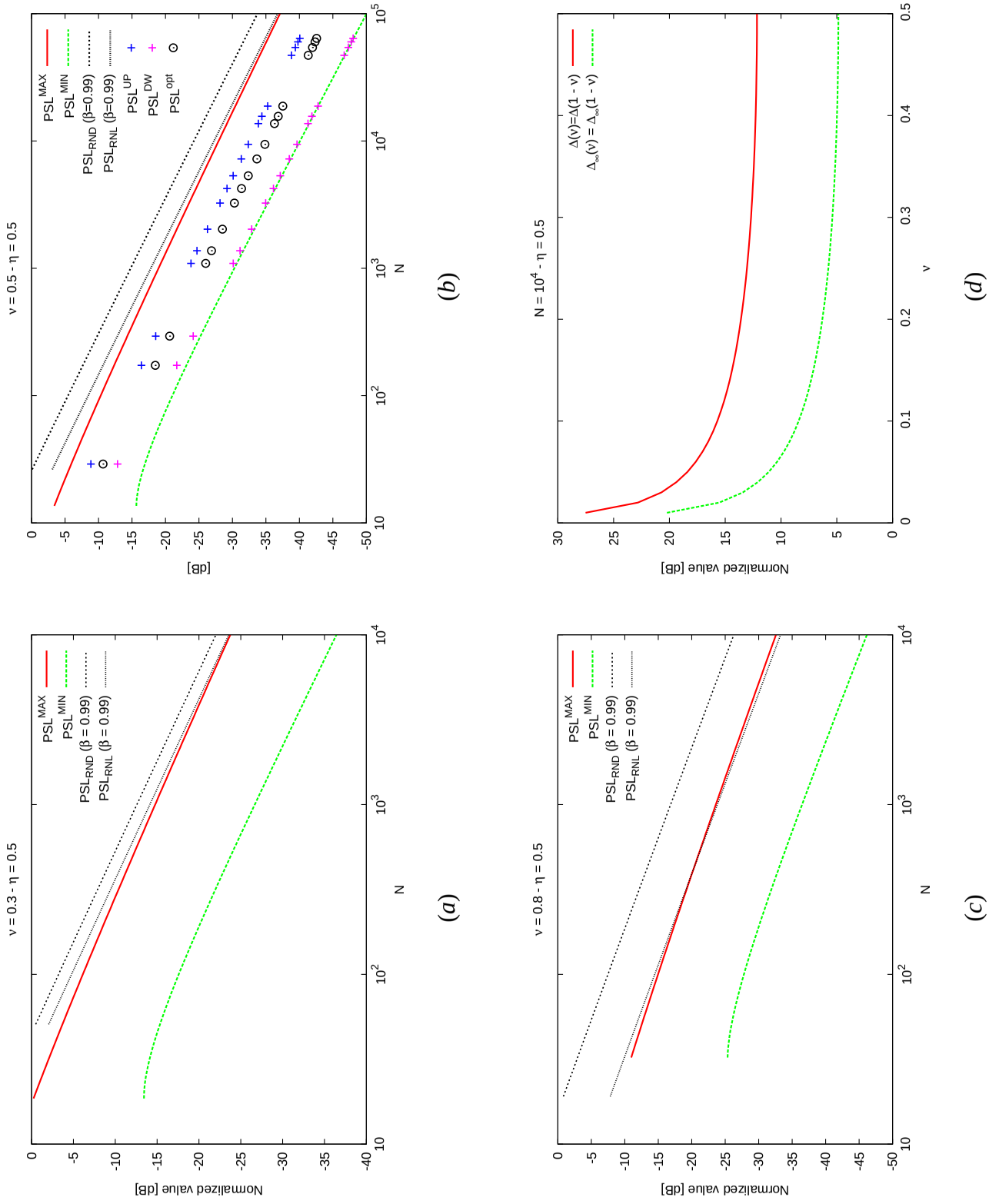

Figure 7 - G. Oliveri et *al.*, “Linear array thinning ...”

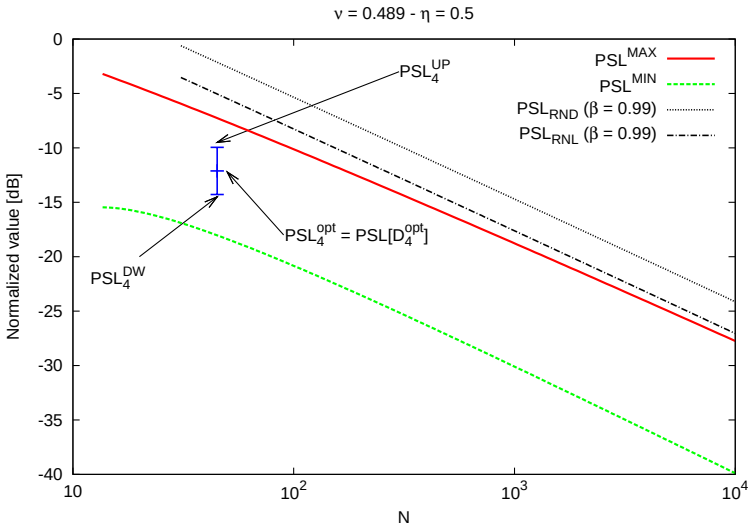

(*a*)

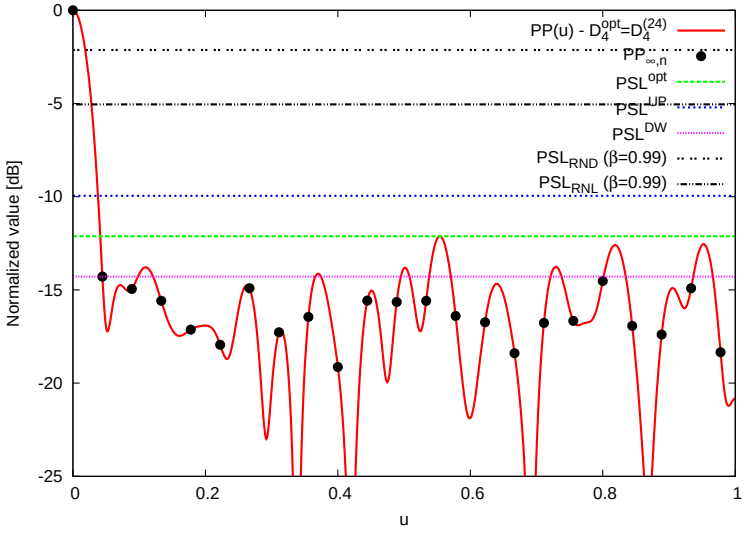

(*b*)

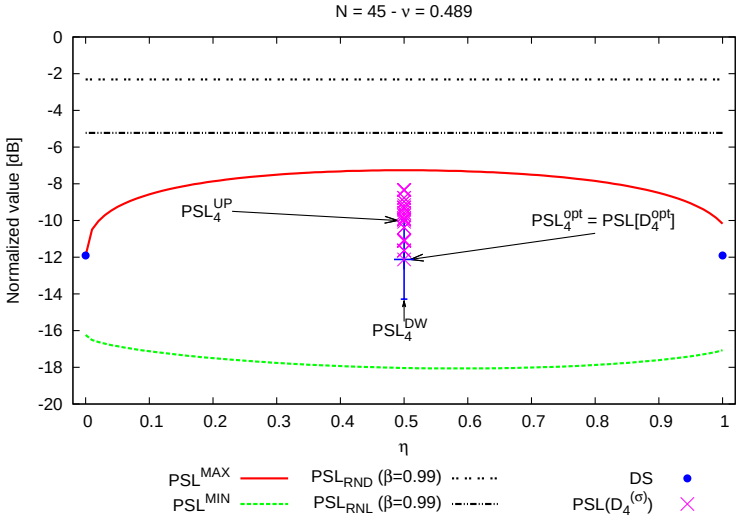

(*c*)

Figure 8 - G. Oliveri et *al.*, "Linear array thinning ..."

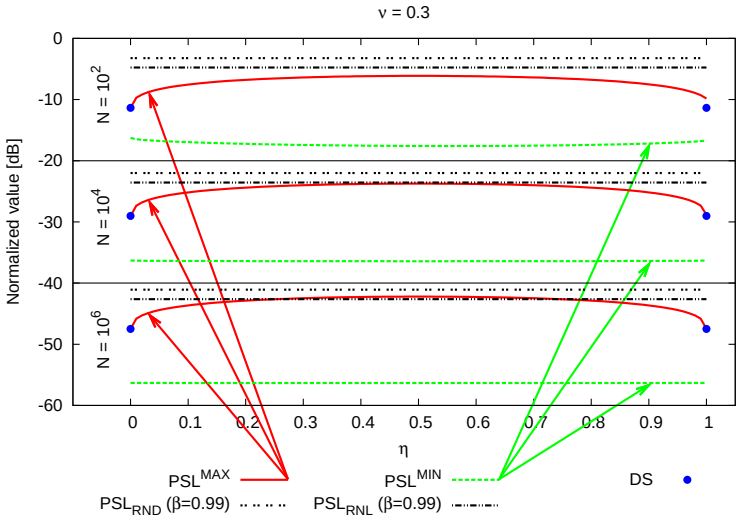

(*a*)

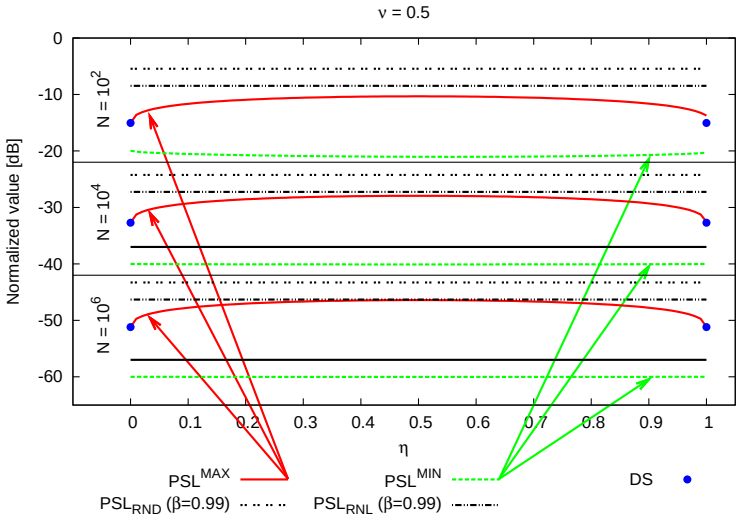

(*b*)

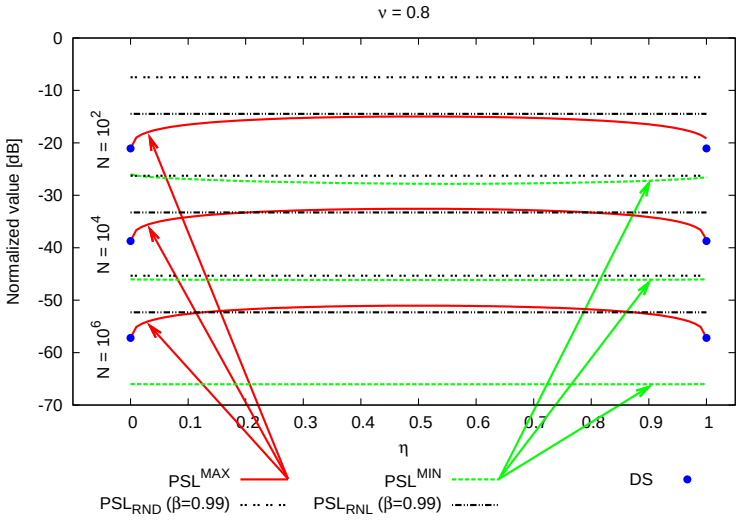

(*c*)

Figure 9 - G. Oliveri et *al.*, “Linear array thinning ...”

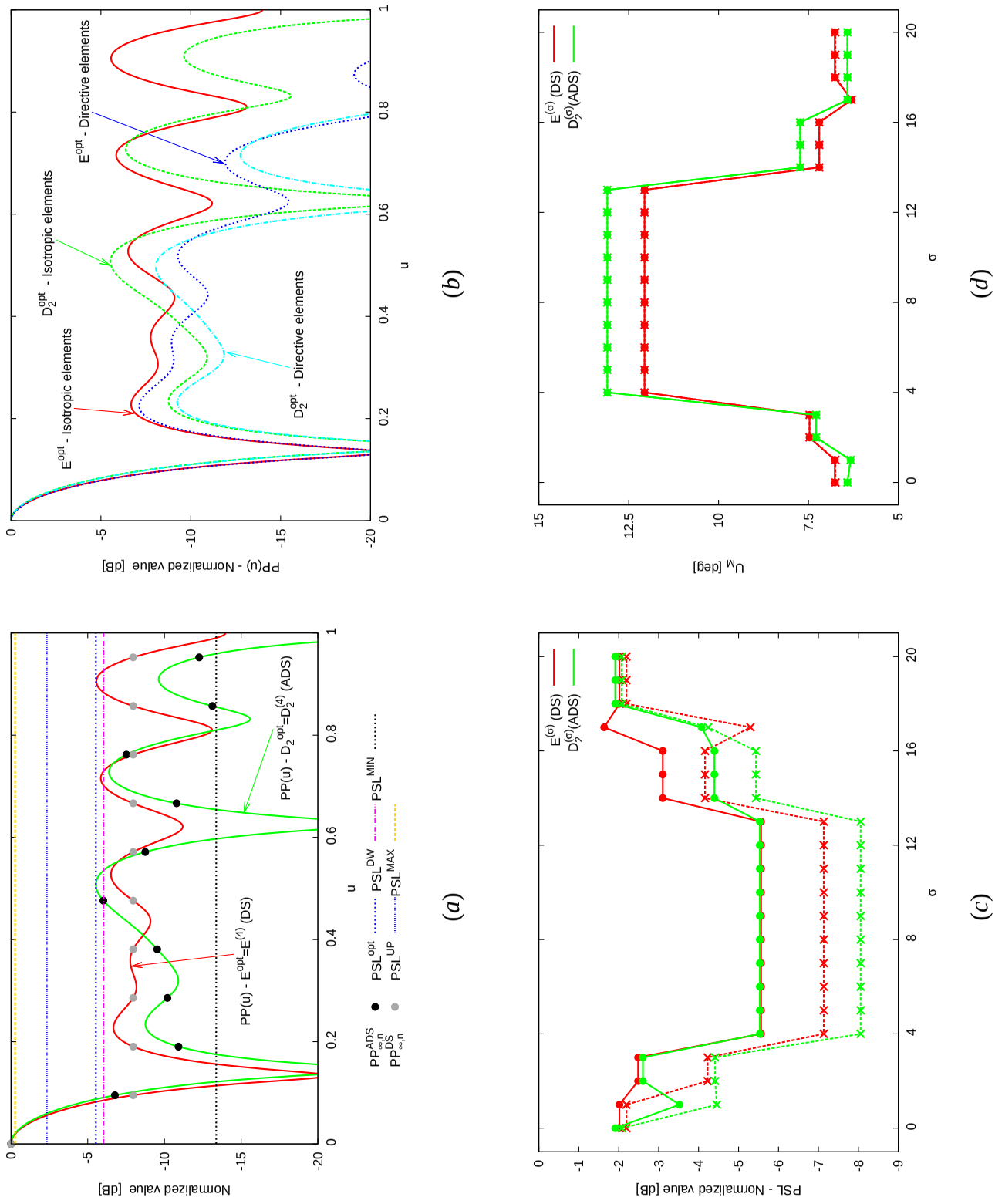

Figure 10 - G. Oliveri et *al.*, "Linear array thinning ..."

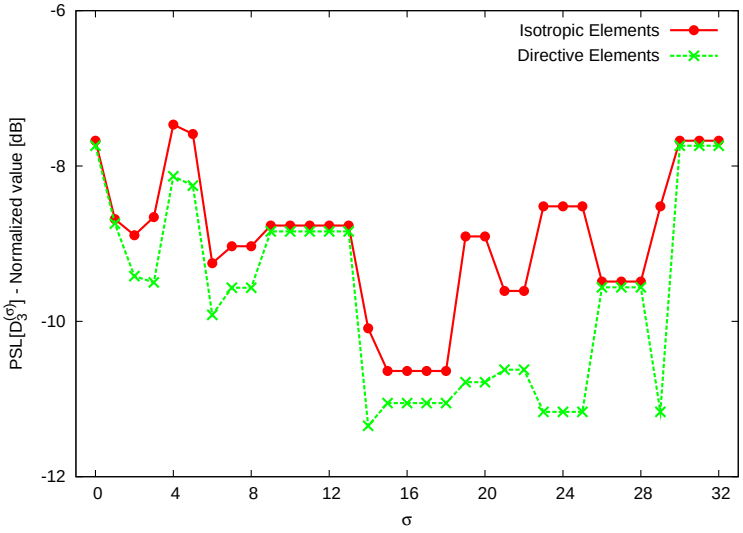

(*a*)

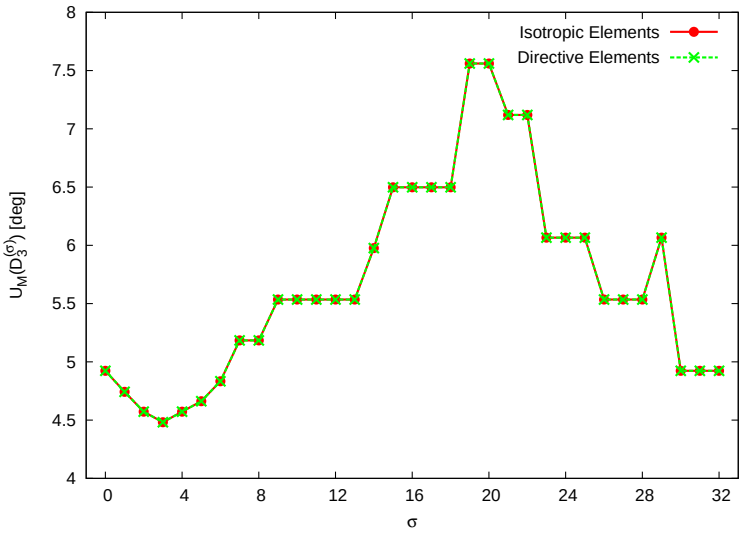

(*b*)

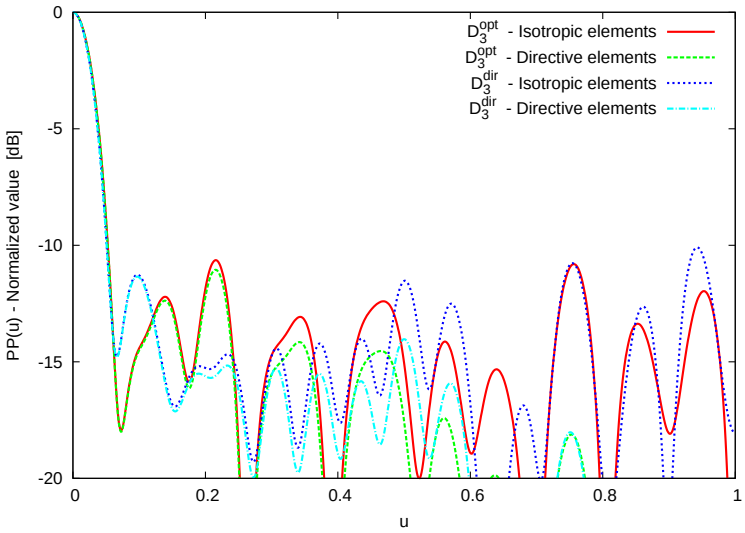

(*c*)

Figure 11 - G. Oliveri et *al.*, “Linear array thinning ...”

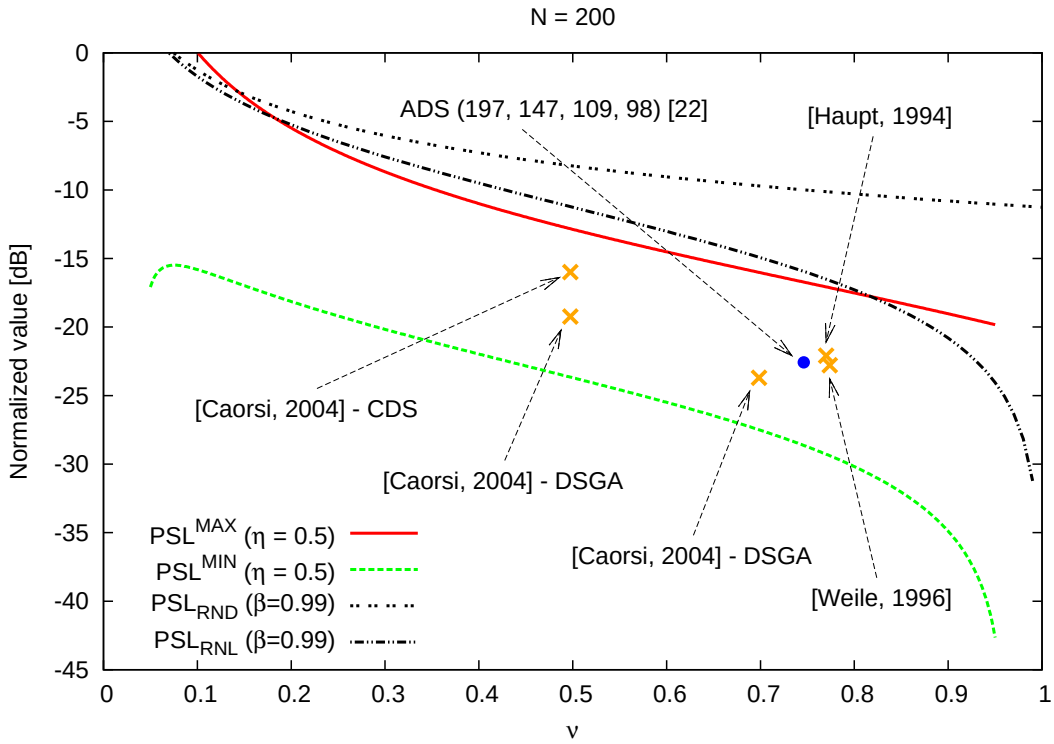

Figure 12 - G. Oliveri et *al.*, "Linear array thinning ..."

Table I - G. Oliveri et *al.*, "Thinned Arrays..."

N	13	21	33	45
$\underline{\mathbf{G}}$	$\underline{\mathbf{G}}_1 = \{0, ..., 12\}$	$\underline{\mathbf{G}}_2 = \{0, ..., 20\}$	$\underline{\mathbf{G}}_2 = \{0, ..., 32\}$	$\underline{\mathbf{G}}_2 = \{0, ..., 44\}$
K	3	6	16	22
Λ	0	1	7	10
t	6	10	16	22
$\underline{\mathbf{D}}$	$\underline{\mathbf{D}}_1 = \{5, 6, 9\}$	$\underline{\mathbf{D}}_2 = \{0, 1, 3, 13$ $16, 17\}$	$\underline{\mathbf{D}}_3 = \{0, 1, 2, 3, 4, 5, 6,$ $8, 13, 14, 18, 20,$ $22, 25, 28, 29\}$	$\underline{\mathbf{D}}_4 = \{0, 1, 2, 3, 4, 5, 6,$ $7, 9, 11, 12, 15,$ $16, 19, 23, 24, 29,$ $30, 32, 35, 37, 39\}$
$\underline{\mathbf{A}}$	$\underline{\mathbf{A}}_1 = \{0000$ 01100 $1000\}$	$\underline{\mathbf{A}}_2 = \{1101000$ 00000010 $0110000\}$	$\underline{\mathbf{A}}_3 = \{11111110100$ 00110001010 $10010011000\}$	$\underline{\mathbf{A}}_4 = \{1111111101$ 01100110010 001100001101 $001010100000\}$
$\underline{\mathbf{S}}$	$\underline{\mathbf{S}}_1 = \{..., \underline{\mathbf{A}}_1, \underline{\mathbf{A}}_1, ...\}$	$\underline{\mathbf{S}}_2 = \{..., \underline{\mathbf{A}}_2, \underline{\mathbf{A}}_2, ...\}$	$\underline{\mathbf{S}}_3 = \{..., \underline{\mathbf{A}}_3, \underline{\mathbf{A}}_3, ...\}$	$\underline{\mathbf{S}}_4 = \{..., \underline{\mathbf{A}}_4, \underline{\mathbf{A}}_4, ...\}$
$C_s^{ADS}(z)$	$3,\ z = 0$ $0,\ z = 2, 5, 6,$ $7, 8, 11$ $1,\ z \in \underline{\mathbf{L}} = \{1, 3,$ $4, 9,$ $10, 12\}$	$6,\ z = 0$ $1,\ z = 2, 6, 7, 9,$ $10, 11, 12,$ $14, 15, 19$ $2,\ z \in \underline{\mathbf{L}} = \{1, 3, 4, 5,$ $8, 13, 16,$ $17, 18, 20\}$	$16,\ z = 0$ $7,\ z = 3, 6, 7, 9, 10, 11,$ $13, 15, 18, 20, 22,$ $23, 24, 26, 27, 30$ $8,\ z \in \underline{\mathbf{L}} = \{1, 2, 4, 5, 8, 12,$ $14, 16, 17, 19, 21,$ $25, 28, 29, 31, 32\}$	$22,\ z = 0$ $10,\ z = 6, 9, 10, 11, 12, 14, 16, 18,$ $19, 20, 21, 24, 25, 26, 27,$ $29, 31, 33, 34, 35, 36, 39$ $11,\ z \in \underline{\mathbf{L}} = \{1, 2, 3, 4, 5, 7, 8, 13, 15,$ $17, 22, 23, 28, 30, 37,$ $38, 40, 41, 42, 43, 44\}$